Chapter

Digital Image Processing Applied to Optical Measurements

Alonso Saldaña-Heredia, Pedro Antonio Márquez-Aguilar, Álvaro Zamudio Lara and Arturo Molina-Ocampo

Abstract

Digital image processing is a useful tool that improves pictorial information for human interpretation and is mainly used for storage, transmission, and representation of different data. In this chapter, we want to introduce an optical technique which couples physical analysis with image processing for a measurement system. Optical methods were used to obtain the stress-strain relation by different invasive and noninvasive methods. This chapter talks about a novel noninvasive methodology to measure stress-strain evolution; this technique is based upon a single laser beam reflected on the cross section of ductile materials (steel and aluminum) while they are under a compression load. The way we measure one laser beam is by using the Gaussian beam propagation equations; we propose that the reflection area of the laser is going to change as the material surface area is compressed and we analyze these differences by using digital image processing. With this technique we are able to construct a stress-strain diagram.

Keywords: compression test, stress-strain, Gaussian beam, Fourier analysis, image processing

1. Introduction

In this chapter, we introduce a new methodology to measure the stress-train relation for ductile materials subjected to a continuum axial load; this loading was carried out by means of a universal testing machine. To obtain the stress-strain relation, materials were submitted to standardized compression tests, and to develop the technique, we used a laser beam impacting the cross section of the materials; the laser reflection was studied through Gaussian beam propagation equations and digital image processing. The scope of the present research is to determine a relation between the free propagation of a Gaussian beam and the stress-strain evolution of a ductile material.

Stress-strain diagrams are very important in understanding the behavior of materials under different loads [1]; these diagrams show the elastic, plastic, and rupture characteristics of materials. There are two methods to obtain these diagrams.

First, the invasive methods from which mechanics draw by doing physical tests, such as the test tube in which a standardized probe is placed on a testing machine; a continuum load is applied to it, and the resulting deformation is measured [2]. Other invasive methods are optical methods, which can determine residual stress, in-field displacements, and strain. Here, hole drilling is the most used technique.

Originally developed in 1930 by Mathar [3], it is nowadays a standardized technique by the ASTM [4].

Second, nondestructive or noninvasive optical methods such as multiple laser displacement sensors which are applied to piping systems [5], stress measurements using crystal curvature technique during film growths [6], and another technique called deflectometry [7, 8], in which light passes through arrays that measure the curvature of objects; they are proposed as mirrors. The reflection caused by these objects is seen in a CCD camera, and the pattern is studied with standard phase shift techniques; most of the used objects are aspherical.

An image was defined as a two-dimensional function: $f(x,y)$ where x and y are plane coordinates and the amplitude f at any pair of coordinates (x,y) is called the intensity referred as a gray level of the image at that point [9]. One of the first applications of digital images was in the newspaper industry through the introduction of the Bartlane cable picture transmission system in the early 1920s, where specialized printing equipment coded pictures for cable transmission and then reconstructed them at the receiving end [9]. However, the image processing method itself required storage and computational power; nevertheless, by this time, it was not possible to talk about processing since the development of the computer hadn't arrived. One of the first works in this field was done by Harry Andrews [10], whom introduced techniques in order to work with images as matrixes; another book about the treatment of pictures was introduced by 1976 [11].

Digital image processing has been applied widely, in such cases as in control level for industries [12], which is based on the treatment of a special light shape generated by a laser, also measuring displacements in infrastructures by a matrix of points [13]. Some researchers around the application in engineering are evaluating the curvature of a pipeline using a parabolic function to determine its deformation [14], analyzing the location of cracks in reinforced concrete by monitoring the surface deformation with two cameras [15], strain measurements during film stretching process following the digital changes of the marker [16], and measuring the strain in time for standardized fatigue tests [17], among others.

In this chapter we introduce a novel methodology to measure the stress-strain behavior of ductile materials; this technique uses a laser beam focused on the cross section of a material probe which is under a compression test. We propose that the materials (1018 steel and aluminum alloy) will act as optical spherical mirrors. This is due to their surface transformation; the laser focuses in a surface which is completely flat, and it will deform as a reaction of the compression test. Therefore, the laser strikes this surface, and acting as a "mirror," it will reflect and scatter the beam. Thus, the reflected laser area will increase as the deformation increases. This laser reflection is analyzed with Gaussian beam propagation equations by using digital image processing to measure each increasing area. This is the procedure we follow to obtain a relation between the laser-beam-free propagation and the strain, which we propose to be similar to the cross-section deformation of both materials. We show the accuracy, error, and sensitivity of the methodology, and we theoretically demonstrate how the laser beam spreads; the present research can be a suitable technique as it only uses a single laser beam for stress-strain characterization.

2. Theory

2.1 Gaussian beam analysis

The Gaussian beam is the simplest, the most known, and the most worked with, because its characteristics and evolution are well-known [18]. The amplitude

function represented from Gaussian beams can be deduced by applying boundary conditions in the optical resonator, where the laser radiation is produced; this amplitude is described by

$$E(x,z) = E_0 \frac{\omega_0}{\omega(z)} \cdot exp\left[\frac{-x^2}{[\omega(z)]^2} - \frac{kx^2}{2R(z)} - kz + \eta(z)\right], \tag{1}$$

where E_0 is the electric field amplitude, ω_0 is the beam waist, $\omega(z)$ is how the beam propagates, k is the wave number ($k = 2\pi/\lambda$), λ is the wavelength, $R(z)$ is the curvature radius of the spherical waves, and $\eta(z)$ is the beam phase angle [19]. Laser beams are able to pass through different media; the light reflection occurs when it arrives to the boundary separating two media of different optical densities, and some of the energy is reflected back into the first medium [20]; taking this outset, if a laser beam strikes a mirror, the reflection can be studied as a Gaussian propagation. In our case, the metallic surface will be modeled as a convex mirror. As it is well-known, there is a relation between the focal length and the curvature radius of a mirror. Using this relation the phase of the transmitted wave is altered to

$$\varphi(x,z) = 2\eta(z) - \frac{kx^2}{z\left(1 + \frac{z_0{}^2}{z^2}\right)} + \frac{kx^2}{f}, \tag{2}$$

where z_0 is the initial Rayleigh distance and f is the focal length of the mirror [21]. To study the propagation through a lens phenomenon, the Gaussian propagation equations are established in which ω_0 and z_0 turns into ω_1 and z_1, respectively, after a distance f and they are calculated by

$$\omega_1 = \frac{\omega_0}{\sqrt{\left(1 + \frac{z_0{}^2}{f^2}\right)}}, \tag{3}$$

$$z_1 = \frac{f}{\left(1 + \frac{f^2}{z_0{}^2}\right)}. \tag{4}$$

This pair of equations involves how Gaussian beam propagates [21], so in order to calculate the new beam waist in the propagation axis, we have

$$\omega(z_p) = \omega_1 \sqrt{\left(1 + \frac{z_p{}^2}{z_1{}^2}\right)}, \tag{5}$$

where $\omega(z_p)$ is the new beam waist at z_p which is the propagation distance.

The goal of this research is to reach a general relation between the strains caused in any material by measuring with one laser beam, its reflection and relating it to a focal length transformation. As we implicate the focal length, we need these Gaussian propagation equations to calculate the changes in the focal length during the compression test. Substituting Eqs. (3), (4) in (5) it can be deduced:

$$\frac{z_p{}^2}{z_0{}^4} \cdot x^2 + x\left(1 - \frac{\omega(z_p)^2}{\omega_0{}^2}\right) - z_0{}^2 = 0. \tag{6}$$

The parameter z_p is calculated doing DIP, taking each area increment per second during the compression test. Once the result from Eq. (6) is obtained, the variation of the focal length is determined applying

$$\xi = \frac{f_f - f_i}{f_i}, \tag{7}$$

where f_f is the final focal length and f_i is the initial focal length; following this procedure, we obtained a dimensionless variable.

2.2 Compression tests

Mechanical tests are used to know the mechanical properties of materials; a compression test enables the user to understand the behavior of a material under a continuum axial load; from this test it is possible to obtain the stress-strain diagram of any material [2]. In this chapter we worked with samples of steel with dimensions of 2.5 × 2.5 × 2.2 cm and aluminum samples of 1 × 1 × 0.9 cm according to the small-type standard dimensions [22]; all samples undergo into compression test according to ASTM E-9 [22]. The tests were performed with a speed ratio of 0.2 cm/s up to 90 MPa for steel and up to 20 MPa for aluminum. Since we are working on the elastic part of the diagram, therefore we can apply Hooke's law:

$$\sigma = E \cdot \varepsilon, \tag{8}$$

where σ is the engineering stress, E is the Young's module of the material (200 and 70 GPa) for steel and aluminum, respectively, and ε is the engineering strain. We propose that the experimental stress is going to behave similar to the Hooke's law; thus, we relate Eq. (8) to the focal length by

$$\sigma = E \cdot K \cdot \xi, \tag{9}$$

where K is a material coefficient proposed in this chapter and ξ is the dimensionless value obtained in Eq. (7). The coefficient K is obtained from the relation between the slopes of both graphs of interest: stress-strain diagram and DIP plot.

2.3 Theoretical analysis

In this research, we used a He-Ne laser with specific parameters such as initial intensity, beam waist, and Rayleigh distance that are shown in its handbook [23].

In **Figure 1** we plot Eqs. (1) and (2) substituting the results from Eq. (7), the initial parameters of our laser and propagating formally this laser beam. In this figure, we can observe that when the focal length increases, the beam waist has also an increase, in this theoretical demonstration; we propose that these increments are proportional as we assume that $\varepsilon \approx f$.

By using Fresnel diffraction and the treatment of lens transmission [24], we have

$$U_f(u,v) = \frac{exp\left[\frac{ik}{2f}\left(u^2+v^2\right)\right]}{i\lambda f} * \iint_{-\infty}^{\infty} U(x,y) \cdot t_A \cdot exp\left[\frac{ik}{2f}(xu+yv)\right] \mathrm{dxdy}, \tag{10}$$

where

$$t_A = exp\left[\frac{ik}{2f}\left(x^2+y^2\right)\right] \tag{11}$$

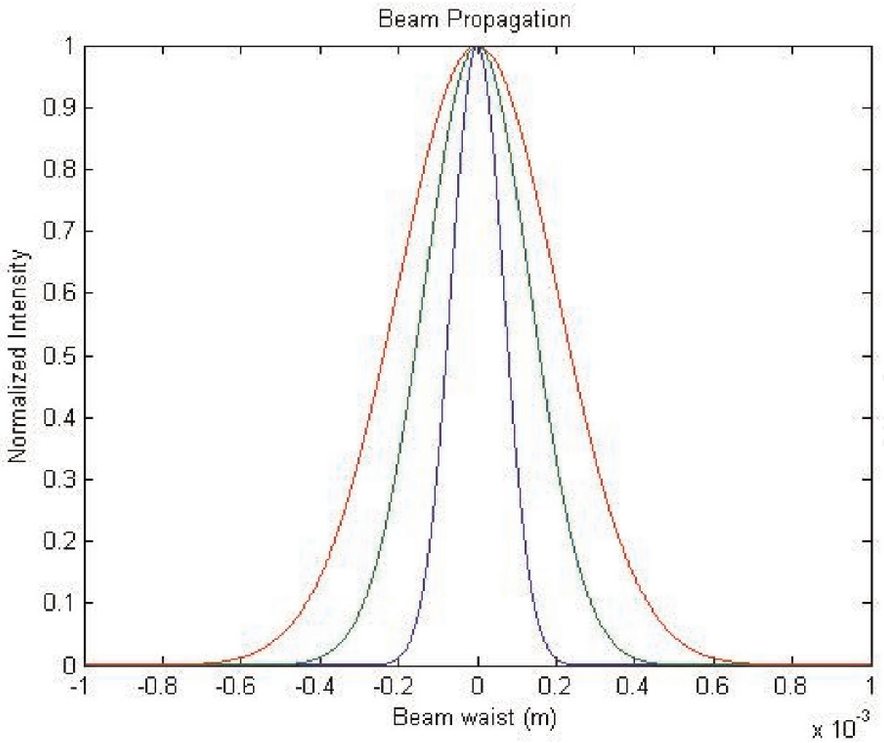

Figure 1.
Gaussian propagation: intensity profile.

and

$$U(x,y) = exp^{-\left[\left(x^2+y^2\right)\right]}. \tag{12}$$

Replacing Eqs. (11) and (12) into Eq. (10), expanding formally and changing coordinates, we obtain

$$U(\rho) = \frac{i\pi}{a\lambda f}\, exp\left[\left(\frac{ik}{2f}+\frac{b^2}{4a}\right)\cdot\rho^2\right], \tag{13}$$

where

$$a = \left(1-\frac{ik}{2f}\right), \tag{14}$$

$$b = \frac{ik}{f}, \tag{15}$$

According to the present research, the initial area of the reflected laser was $A \sim 0.009\ m^2$.

3. Methodology

As we established before, we use two ductile materials: steel and aluminum; in total, seven samples were hand-sanded and polished in the same manner to mirror grade in the laser-impact section, and they were placed in the machine perpendicular to the piston to begin the compression test. A diagram of this method is shown schematically in **Figure 2a**. The output of a He-Ne laser (L), with a wavelength

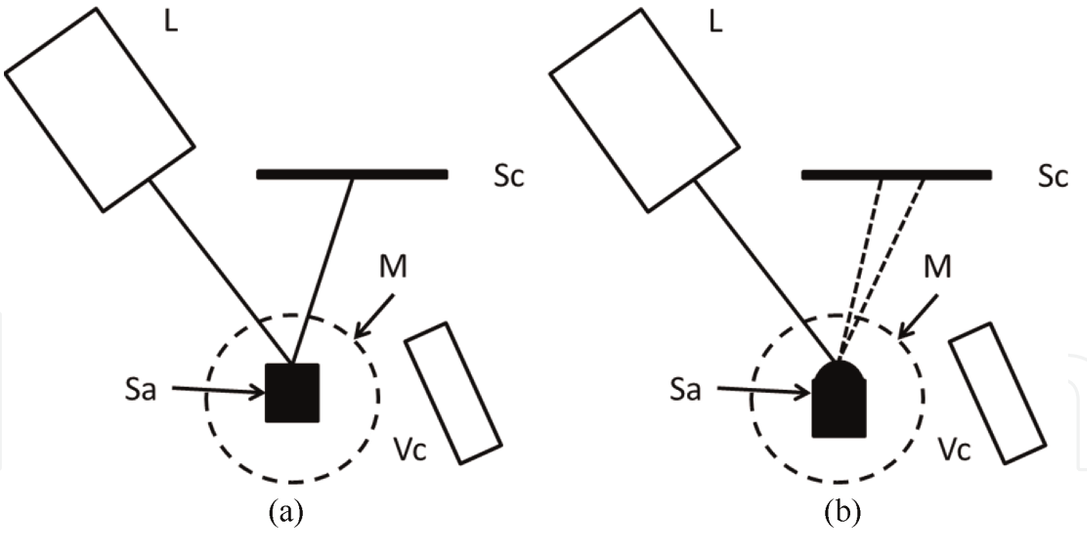

Figure 2.
Experimental setup: (a) material with no strain; (b) the strained material will scatter light.

λ = 632 nm and a power of 1 mW, is placed 15 cm from the sample (Sa) in order to irradiate the polished face, and then, the reflected beam impacts a screen (Sc) which is placed 10 cm beside the laser beam and parallel to the sample. The material is first completely flat, with no stress, and as it is compressed with the universal machine (M), the size of the cross section will decrease as a reaction (**Figure 2b**). During the tests, the deformation rate was 0.2 cm/s with duration of 5 min approximately, and while they were taking place, the reflected light was recorded with a video camera (Vc) which is placed in front and parallel to the screen aside the sample. All tests were done at room temperature, and samples were compressed around 2 mm.

When we finish the mechanical test, a post-processing is carried out:

1. First, we need to transfer the video from the video card to the computer.

2. Then, we use the free software called *Video to JPG converter*; it helps us to divide the entire video into each frame. The software enabled us to turn our videos with an average of 54 frames per second.

3. A program is written in Matlab® for digital image processing.

To do the image processing, we used some Matlab® toolbox functions, mention, and describe them:

- *imread*: this function loads the image as a matrix.
- *rgb2grey*: this code turns the colored image into a gray scale level.
- *im2bw*: this is necessary to convert the image matrix into a binary code.
- *bwarea*: we call this function at the end of the code to calculate by binary code the total area of the reflected laser beam.

Along **Figure 3**, we can observe how the code works: in **Figure 3a** it is seen how *imread* works; when we call it, the image is loaded; for **Figure 3b** we can observe how *rgb2grey* converts the colored image into a grayscale; in **Figure 3c** we called

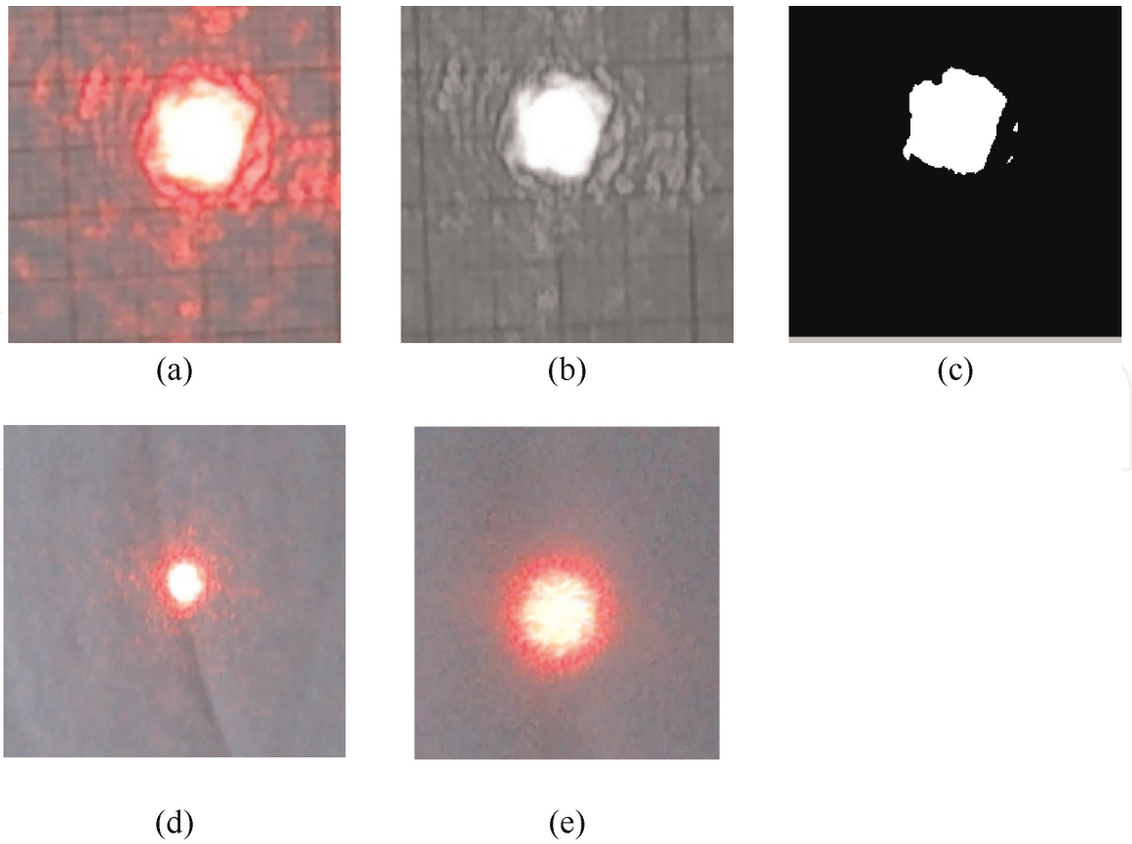

Figure 3.
Image processing: (a) how the image is loaded; (b) grayscale image; (c) binary image; (d) initial beam diameter; (e) beam diameter at $t = t_i + \Delta t$.

im2bw to do a binary code of the image. At this step we can apply the function *bwarea* to know the area of this "circle." We can observe in **Figure 3d** and **e** how the beam diameter increases, for a $t_i = 0$ s and $t_f = \Delta$t s. By following the methodology described and using Eq. (6), we can obtain the change in the focal length and relate it to the deformation in the material.

The code was written to repeat this process iteratively for every image. We propose that the calculated area is the parameter $\omega(z_p)$. Therefore Eq. (6) is used to calculate the focal length. We know that as a result of doing a mechanical test, we can obtain a stress-strain diagram; it is calculated through strain gages and special software incorporated to the machine. At the end of the iterative process, we plot the focal length differences following Eq. (7).

4. Results

Along this chapter, we have mentioned that we prepared four steel samples and three aluminum probes, to test them under standardized compression test; for each one we obtained two graphs of interest, the stress-strain diagram and the DIP plot; **Figure 4** shows these two graphs of interest. **Figures 4–8** correspond to steel samples.

In **Figure 4a** we show the stress-strain diagram obtained from the software of the machine; in **Figure 4b** we can observe the related stress-focal length diagram obtained by following the experimental procedure and using Eq. (9). In the graphs we can observe a linear behavior. In section 2.2, we propose an equation related to Hooke's law, where the K value is calculated using the slopes of each graph and $\Delta\varepsilon$ is taken from 0.1 to 0.3%ε. Therefore the calculated slope of the real stress-strain

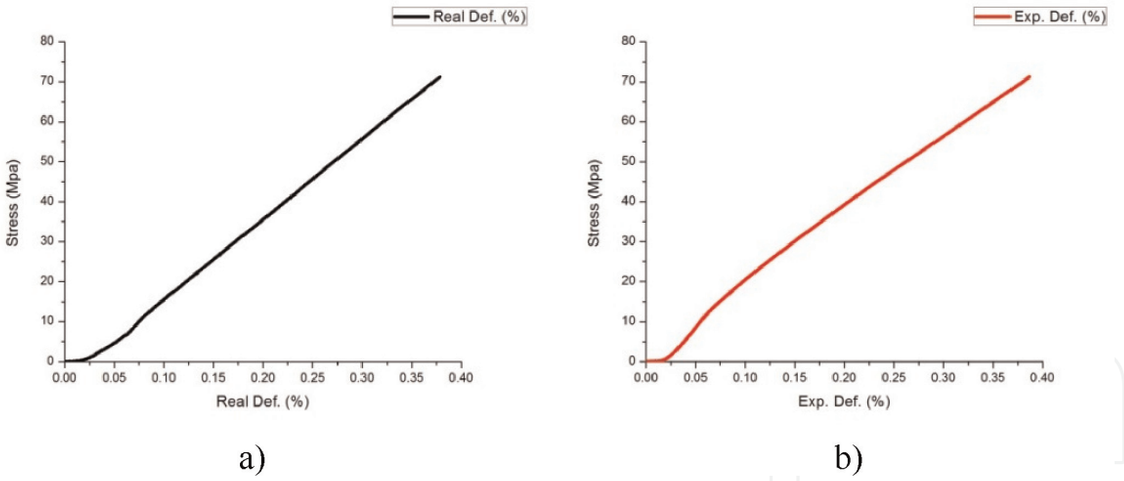

Figure 4.
Stress-strain diagrams: (a) obtained from universal machine, (b) experimentally from optical treatment.

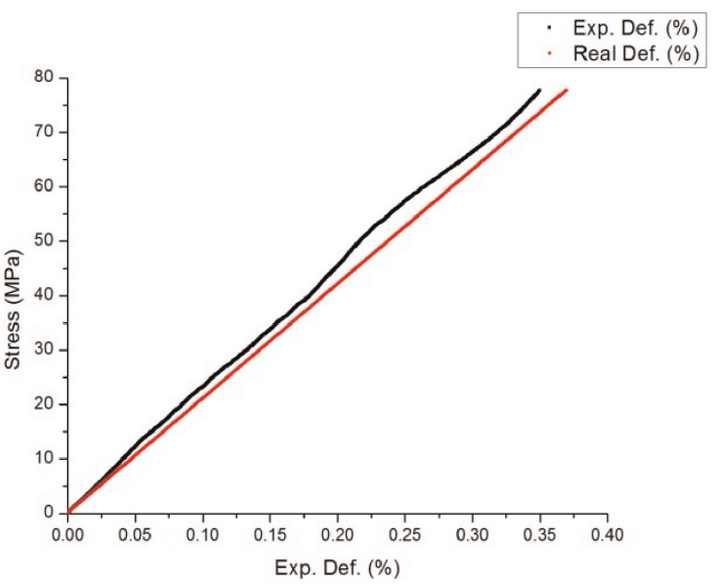

Figure 5.
Comparison between stress-strain diagrams for steel's sample 1.

diagram is 0.00351 and for the experimental data is 0.001401; *K* coefficient between them is 2.5.

In **Figure 5** we show the first steel sample comparison between the real strain (Real Def.) and the experimental related-strain (Exp. Def.); both are represented in % as strain has no dimensions, and also some statistical results are shown in **Table 1**. From here, the following graphs are going to be presented the same way.

We repeat this procedure for the next three samples, obtaining *K* factor and comparing the real stress-strain diagram with the experimental plot and showing the statistical results for each one.

For the second test, we can see in **Table 2** that *K* factor remains in a value of 2.5; in this test we obtained an accurate result of 88% as compared to the real graph. In the third and fourth tests, we see in **Tables 3** and **4** that the value of the proposed *K* factor decreases to 2.4, but we obtained the same approach in reproducing the stress-strain diagram.

In **Figures 5** and **7**, the behavior of the experimental graph is above the real stress-strain diagram; for **Figures 6** and **8**, the behavior has an intersection—it first starts below then crosses above it. We propose that the behavior of the area increase

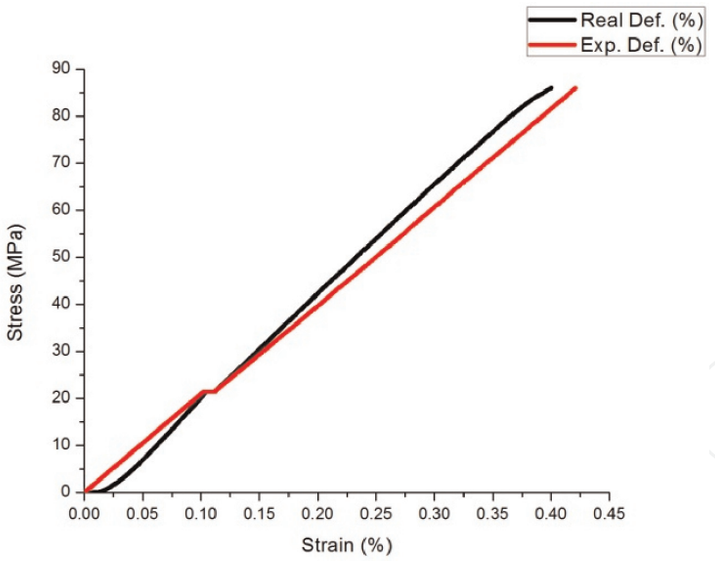

Figure 6.
Comparison between stress-strain diagrams for steel's sample 2.

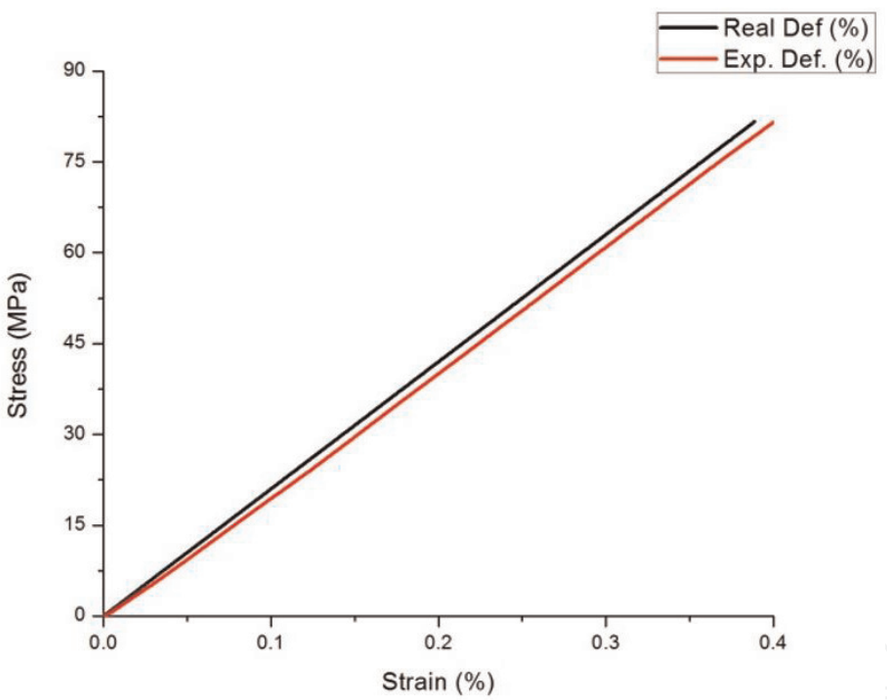

Figure 7.
Comparison between stress-strain diagrams for steel's sample 3.

is due to the material surface, as it was hand-sanded and polished; light is not reflecting equally in every sample of material.

In **Table 5** we summarize the accuracy and mean error for this four strain measurements; we can observe that the mean accuracy of our methodology is 89%.

With this novel technique, taking the focal length as a parameter for measuring the stress-strain relation of a material, we proved an 89% effectiveness following standardized compression tests using steel samples; also we obtained a K value for this material of 2.5, which establishes the relation between the slopes of the real and the experimental graphs [25].

In this section, we present the statistical results and stress-strain diagrams obtained from aluminum samples. We are following the same process by comparing the DIP graph with the real stress-strain obtained from the universal machine

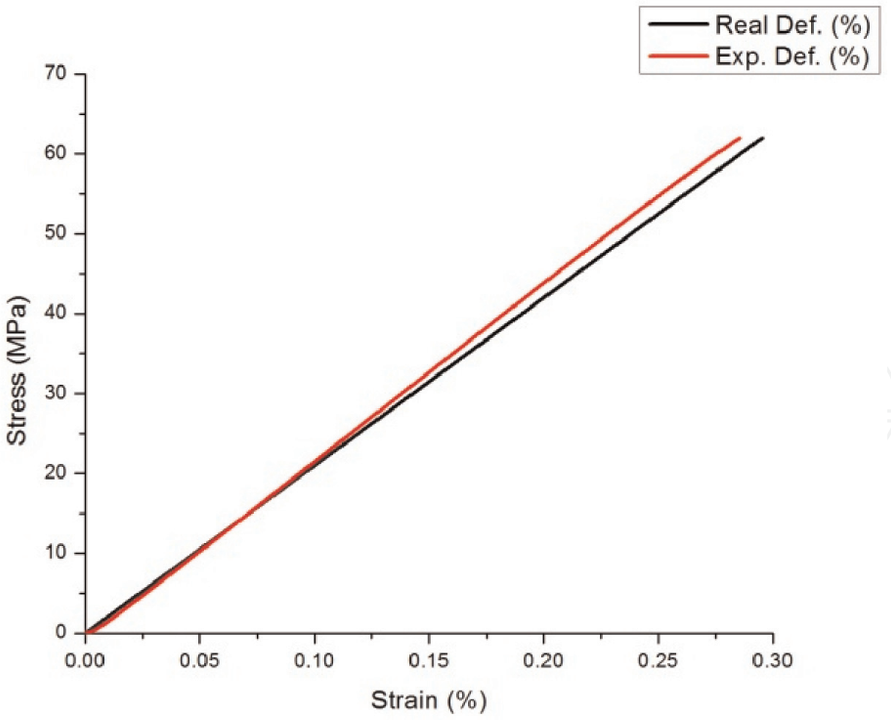

Figure 8.
Comparison between stress-strain diagrams for steel's sample 4.

First sample	
K factor	2.5
Young's modulus E	188 ± 12 GPa
% difference from 200 GPa	11%
Standard deviation	0.011

Table 1.
Statistical result for steel's sample 1 during the compression tests and Gaussian beam analysis.

Second sample	
K factor	2.5
Young's modulus E	188 ± 12 GPa
% difference from 200 GPa	11%
Standard deviation	0.010

Table 2.
Statistical results for steel's sample 2 during the compression tests and Gaussian beam analysis.

Third sample	
K factor	2.4
Young's modulus *E*	188 ± 12 GPa
% difference from 200 GPa	11%
Standard deviation	0.012

Table 3.
Statistical results for steel's sample 3 during the compression tests and Gaussian beam analysis.

Fourth sample	
K factor	2.4
Young's modulus *E*	187 ± 13 GPa
% difference from 200 GPa	11%
Standard deviation	0.013

Table 4.
Statistical results for sample 4 during the compression tests and Gaussian beam analysis.

Sample	**Accuracy (%)**	***K***
1	89	2.5
2	89	2.5
3	89	2.4
4	89	2.4

Table 5.
Accuracy and error of the four tests.

software. **Figure 9** and **Table 6** show the results for the first aluminum sample; with this material we obtained a *K* value of 4.52 and an approach of 90%.

Using aluminum samples, we obtained similar approximations to the steel ones. In **Table 7** we can observe a *K* value of 4.54 and a slightly less approach than sample 1, obtaining 89%. In **Table 8** we observe a *K* value of 4.5 and an approach of 88%.

By comparing **Figures 9–11** to steel results, we can see that aluminum alloys behave differently than steel ones. In these figures we can appreciate that the experimental graph goes above the real diagram at the same point (0.08%). In **Figures 10** and **11**, the experimental result goes first below, then above the real stress-strain diagram. These differences, such as steel ones, are due to the sample surface; during the process of making mirror-grade samples, we can accidentally cause nonuniform surfaces, and thus light reflection is not always the same.

In **Table 9** we summarize the accuracy and mean error for these three measurements; it is seen that the mean accuracy of our method is 89%.

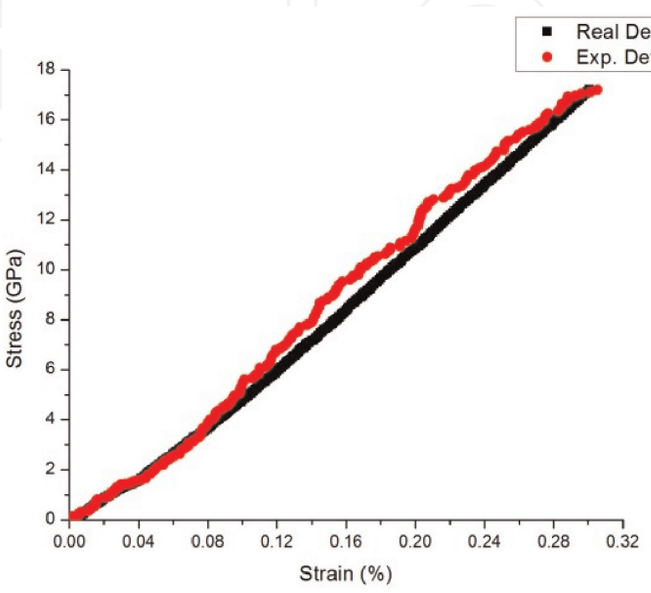

Figure 9.
Comparison between stress-strain diagrams for aluminum's sample 1.

First sample	
K factor	4.52
Young's modulus *E*	63 ± 7 GPa
% difference from 70 GPa	10%
Standard deviation	0.015

Table 6.
Statistical results for aluminum's sample 1 during the compression tests and Gaussian beam analysis.

Second sample	
K factor	4.54
Young's modulus *E*	62 ± 8 GPa
% difference from 70 GPa	11%
Standard deviation	0.013

Table 7.
Statistical results for aluminum's sample 2 during the compression tests and Gaussian beam analysis.

Third sample	
K factor	4.5
Young's modulus *E*	61 ± 9 GPa
% difference from 70 GPa	12%
Standard deviation	0.018

Table 8.
Statistical results for aluminum's sample 3 during the compression tests and Gaussian beam analysis.

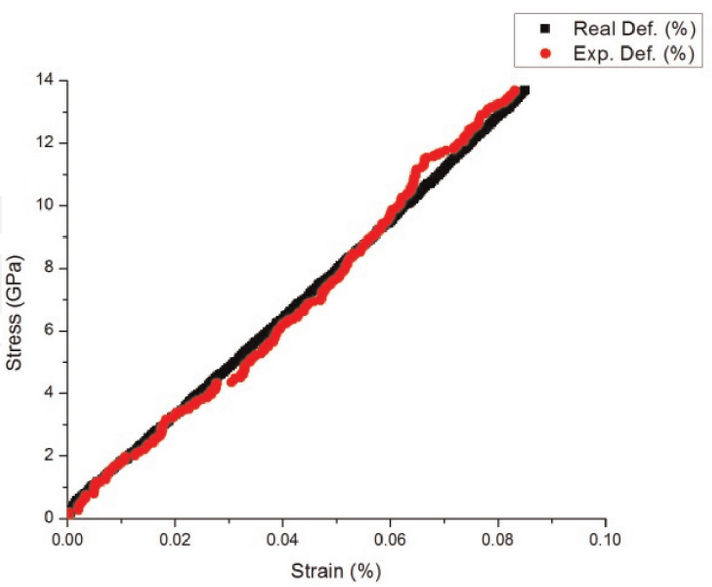

Figure 10.
Comparison between stress-strain diagrams for aluminum's sample 2.

With this developed technique, taking the focal length as a parameter for measuring the stress-strain relation of a material, we proved an 89% effectiveness following standardized compression tests using aluminum samples; we also obtained a *K* value for this material of 4.5, which stablishes the relation between the slopes of the real and the experimental graphs [26].

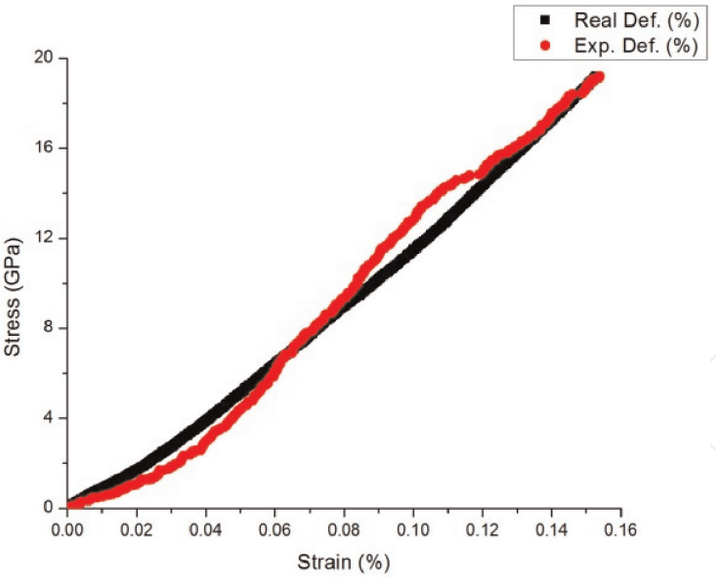

Figure 11.
Comparison between stress-strain diagrams for aluminum's sample 3.

Probe	Accuracy (%)	*K*
1	90	4.54
2	89	4.52
3	88	4.5

Table 9.
Accuracy and error of the three tests.

Summarizing these tests, steel and aluminum, we observed that the present methodology can measure the stress-strain relation of a ductile material with an average error of 11%. We established that by recording the video, we obtained 54 images in average; therefore, we calculate the mean differences between measurement in a 10-s time interval, thus to obtain the sensitivity of this methodology, which resulted to 27 microdeformations.

5. Conclusion

The stress-strain relation of two ductile materials under standardized compression test was measured using one laser beam, its reflection, and digital image processing treatment; we obtained 89% of accuracy and a relation of 27 microdeformation. Also it was demonstrated that the diameter of the laser reflection has an increment according to the increase in the focal length; we also showed following Fresnel diffraction and the transmission through a lens that the comparison between the reflected area and the experimental results is congruent.

Acknowledgements

Alonso Saldaña Heredia wants to thank CONACYT for the grant no. 360140.

Conflict of interest

The authors declare no conflict of interest for this chapter.

Author details

Alonso Saldaña-Heredia[1*], Pedro Antonio Márquez-Aguilar[2], Álvaro Zamudio Lara[2] and Arturo Molina-Ocampo[2]

1 Metropolitan Polytechnic University of Hidalgo—UPMH, Tolcayuca, Mexico

2 Research Center on Engineering and Applied Sciences—IICBA, Autonomous University of Morelos State, Cuernavaca, Mexico

*Address all correspondence to: aheredia@upmh.edu.mx

References

[1] Figliola R, Beasley F. Theory and Design for Mechanical Measurements. 5th ed. USA: John Wiley & Sons; 2011. 605 p. ISBN: 978-0-470-54741-0

[2] Gere J, Goodno B. Mecánica de Materiales. 8th ed. Cengage Learning: Mexico; 2016. 1125 p. ISBN: 978-1-111-57773-5

[3] Mathar J. Determination of initial stresses by measuring the deformation around drilled holes. Transactions of the ASME. 1934;**56**(4):249-254

[4] ASTM. Determining residual stresses by the hole-drilling strain gage method. In: ASTM Standard Test Method E837-08. West Conshohocken, PA: American Society for Testing and Materials; 2008

[5] Maekawa A et al. Development of noncontact measurement methods using multiple laser displacement sensors for bending and torsional vibration stresses in piping systems. International Journal of Pressure Vessels and Piping. 2015;**137**:38-45. DOI: 10.1016/j.ijpvp.2015.05.002

[6] Premper J et al. In situ stress measurements during pulsed laser deposition of $BaTiO_3$ and $SrTiO_3$ atomic layers on Pt(0 0 1). Applied Surface Science. 2015;**335**:44-49

[7] Liu Y et al. Fast and accurate deflectometry with crossed fringes. Advanced Optical Technologies. 2014;**3**(4):441-445

[8] Huang E et al. Measuring aspheric surfaces with reflection deflectometry. SPIE Newsroom. 2013. 3 p. DOI: 10.1117/2.1201309.005087. Available from: https://www.researchgate.net/publication/275085156_Measuring_aspheric_surfaces_with_reflection_deflectometry/link/554d1c9f0cf21ed2135f5dca/download

[9] González R, Woods R. Digital Image Processing. 2nd ed. New Jersey: Prentice Hall; 2002. 793 p. ISBN: 978-0-201-18075-6

[10] Andrews HC. Computer Techniques in Image Processing. NY: Academic Press; 1970

[11] Rosenfeld A, Kak CA. Digital Picture Processing. NY: Academic Press; 1982

[12] Li C et al. Digital image processing technology applied in level measurement and control system. Procedia Engineering. 2011;**24**:226-231

[13] Kim S-W, Kim N-S. Multi-point displacement response measurement of civil infrastructures using digital image processing. Procedia Engineering. 2011; **14**:195-203

[14] Iwamoto T, Kanie S. Evaluation of bending behavior of flexible pipe using digital image processing. Procedia Engineering. 2017;**171**:1272-1278

[15] Rimkus A et al. Processing digital images for crack localization in reinforced concrete members. Procedia Engineering. 2015;**122**:239-243

[16] Muniandy K et al. Online strain measurement during blown film extrusion using digital image correlation. Journal of Mechanical Engineering. 2018;**5**:154-165

[17] Blug A et al. Real-time GPU-based digital image correlation sensor for marker-free strain-controlled fatigue testing. Applied Sciences. 2019;**9**:1-15

[18] Alda J. Laser and Gaussian beam propagation and transformation. Encyclopedia of optical Engineering.

2003. 16 p. Available from: https://www.researchgate.net/publication/255041663_Laser_and_Gaussian_Beam_Propagation_and_Transformation/link/00463522b465e900a9000000/download

[19] Yariv A. Quantum Electronics. 3rd ed. U.S.A.: John Wiley & Sons; 1990. 693 p. ISBN: 978-0-471-60997-1

[20] Wood R. Physical Optics. 3rd ed. Washington DC: Optical Society of America; 1988. 846 p. ISBN: 155-752-0631

[21] Saleh AEB, Teich MC. Fundamentals of Photonics. 1st ed. New York: John Wiley & Sons; 1991. 982 p. ISBN: 978-0-585-32147-9

[22] ASTM E-9, ICS Number Code 77.040.10 (Mechanical testing of metals). DOI: 10.1520/E0009-09

[23] JDSU Self-Contained Helium-Neon Laser Systems 1500 series Specification Sheet. JDS Uniphase Corporation 10138846 005 0512 SCHNL1500.DS.CL.AE. 2012

[24] Goodman JW. Introduction to Fourier Optics. 3rd ed. United States: Roberts & Company; 2005. 509 p. ISBN: 0-9747077-2-4

[25] Saldaña HA, Márquez APA, Molina OA. Laser-beam reflection for steel stress-strain characterization. Measurement. 2018;**113**:92-98

[26] Saldaña HA, Márquez APA, Molina OA. Aluminum strain measurement by beam propagation. In: Martínez-García A et al., editors. Emerging Challenges for Experimental Mechanics in Energy and Environmental Applications. Proceedings of the 5th International Symposium on Experimental Mechanics and 9th Symposium on Optics in Industry (ISEM-SOI), Conference Proceedings of the Society for Experimental Mechanics Series. 2015. DOI: 10.1007/978-3-319-28513-9_2